

論文 / 著書情報
Article / Book Information

Title	Microfluidic generation of monodispersed Janus alginate hydrogel microparticles using water-in-oil emulsion reactant
Authors	Yingzhe Liu, Takasi Nisisako
Citation	Biomicrofluidics, Vol. 16, Issue 2,
Pub. date	2022, 3
Note	This article may be downloaded for personal use only. Any other use requires prior permission of the author and AIP Publishing. This article appeared in Biomicrofluidics, Vol. 16, Issue 2, and may be found at https://doi.org/10.1063/5.0077916 .

This is the author's peer reviewed, accepted manuscript. However, the online version of record will be different from this version once it has been copyedited and typeset.
PLEASE CITE THIS ARTICLE AS DOI: 10.1063/1.50077916

Microfluidic generation of monodispersed Janus alginate hydrogel microparticles using water-in-oil emulsion reactant

Yingzhe Liu^a and Takasi Nisisako^{b*}

^aDepartment of Mechanical Engineering, School of Engineering, Tokyo Institute of Technology, Tokyo, Japan

^bInstitute of Innovative Research, Tokyo Institute of Technology, R2-9, 4259 Nagatsuta-cho, Midori-ku, Yokohama, Kanagawa, 226-8503 Japan

***Correspondence author:**

E-mail: nisisako.t.aa@m.titech.ac.jp

Tel.: +81-45-924-5092

ABSTRACT

Microparticles with uniform anisotropic structures are widely used in physical, chemical, and biological fields owing to their ability to combine multiple functions on a micro-scale. Here, a microfluidic emulsion-based external gelation (μ FEEG) method was demonstrated for the first time to produce monodisperse Janus calcium alginate (Ca-alginate) hydrogel microparticles consisting of two compartments. This approach provided a fast reaction condition under which we could prepare magnetic Janus Ca-alginate microparticles with diameters ranging from 148 to 179 μm and a coefficient of variation (CV) less than 4%. Moreover, the boundaries between the two compartments were clear. In addition, the volume fraction of each compartment could be adjusted by varying the flow rate ratio between two dispersed phases. Next, we produced fluorescent Janus beads and magnetic-fluorescent Janus beads with an average diameter of ~ 150 μm (CV $< 4.0\%$). The magnetic Janus hydrogel microparticles we produced could be manipulated by applying a magnetic field to achieve self-assembly, rotation, and accumulation. Magnetic Janus hydrogel microparticles are also capable of mammalian cell encapsulation with good cell viability. This paper presents a simple and stable approach for producing monodisperse bi-compartmental Janus hydrogel microparticles that could have great potential for application in physical, biochemical, and biomedical fields.

Keywords: Microfluidics; Janus microparticles; Alginate hydrogel; External gelation; Magnetism; Cell encapsulation

I. INTRODUCTION

“Janus” particles are particles that have bi-compartmental structures of physical and/or chemical anisotropy¹⁻⁴. Janus microbeads can be used to construct self-assembled materials⁵, tissue structures⁶, drug delivery vehicles⁷, optical devices⁸ and electronic papers⁹, that cannot be realized by the isotropic type. Among the various types of Janus beads, microparticles with asymmetric magnetic and/or fluorescent properties have drawn extensive attention. Magnetic Janus particles that have the ability to be handled remotely can be used as micro-rheological probes^{10,11}, micro-motors^{12,13}, components of twisting-ball display^{9,14}, capsules in cell culturing^{15,16}, and for detecting biomolecules^{17,18}. Fluorescent Janus particles with good photo-stability and sharp fluorescence peaks are excellent probes for in vivo targeting¹⁹ and bio-labeling²⁰. In addition, Janus particles with fluorescent and magnetic anisotropy in separated compartments can be used for magnetic field modulated imaging and have a great potential in cancer therapeutics²¹⁻²³.

Commonly, functional nanoparticles (e.g., Fe₃O₄ or quantum dots) are combined with polymer materials to generate magnetic and/or fluorescent Janus beads. Typical approaches to fabricate Janus particles with magnetic and/or fluorescent anisotropy include mask templating²⁴, flame synthesis²⁵, phase separation²⁶, electrodynamic jetting²⁷ as well as microfluidics^{9,14-18,28-33}. Among these techniques, microfluidic approaches have irreplaceable advantages as they can prepare Janus particles with high monodispersity through a simple and scalable process. To date, various methods have been reported for synthesizing magnetic and fluorescent Janus particles using droplet microfluidics (**Table S1**). Using these methods, magnetic and/or fluorescent Janus microbeads were made from materials such as alginate^{15,16,18,32,33}, poly(*N*-isopropylacrylamide)^{14,30}, poly(ethylene glycol)-diacrylate^{17,29}, acrylamide monomer⁹, poly(methyl methacrylate)²⁸, and ethoxylated trimethylolpropane triacrylate³¹.

Alginate is a widely used polysaccharide that can be extracted from brown algae³⁴. Biocompatibility, nontoxicity, and biodegradability of alginate makes it suitable for diverse biological applications. To

date, several studies that use continuous microfluidic external gelation for synthesizing magnetic and/or fluorescent Janus alginate hydrogel particles have been reported. For example, Zhao et al.¹⁶ prepared magnetic Janus alginate gel beads through the microfluidic generation of a Janus sodium-alginate (Na-alginate) droplet and a calcium chloride (CaCl_2) droplet and their 1:1 pair coalescence in a downstream channel. However, this method requires precise control over the flow rates to generate the two droplets synchronously and to induce their coalescence downstream. Furthermore, Lan et al.¹⁸ and Li et al.³² generated magnetic and fluorescent Janus alginate hydrogel particles by introducing an oil phase containing calcium ions (Ca^{2+}). Nevertheless, this method requires the laborious sample preparation steps because of the low solubility of Ca^{2+} in the oil phase. Instead, Zhang et al.³⁵ developed a continuous internal gelation method to generate monodisperse fluorescent Janus alginate gels with an average diameter below 100 μm with clear interfaces using calcium-ethylenediaminetetraacetic acid (Ca-EDTA) as the reactant. However, an acid oil phase was required to trigger the cross-linking reaction. Hence, the particles must be separated from the oil phase as soon as possible to avoid possible cytotoxicity when used for cell encapsulation. In contrast, Maeda et al.¹⁵ and Yoshida et al.³³ reported centrifugal force-based batch processes for synthesizing monodisperse magnetic and fluorescent Janus alginate gels (average diameter: $\sim 100 \mu\text{m}$, coefficient of variation: $<4\%$) with a clear interface by first forming the precursor Janus alginate droplets in the air and subsequently introducing them into the aqueous phase where gelation is initiated. Aketagawa et al.³⁶ obtained magnetic Janus alginate beads with sizes $<50 \mu\text{m}$ through a semi-batch shrinkage-gelation process. However, noncontinuous production is a major limitation of these two methods. To the best of our knowledge, a microfluidic emulsion-based continuous external gelation method that can produce monodisperse and highly spherical Janus Ca-alginate hydrogel microparticles with a clear interface has never been reported.

In this paper, we present an acid-free microfluidic emulsion-based external gelation (μFEEG) method³⁷ that continuously produces monodisperse and highly spherical Janus calcium alginate (Ca-

alginate) microspheres with magnetic and/or fluorescent anisotropies. When Janus Na-alginate droplets came in contact and merged with fine calcium chloride (CaCl_2) emulsion drops, the supplied Ca^{2+} ions rapidly crosslink the alginate network by the ion-exchange reaction to form Janus hydrogel beads with clear interfaces before possible convective and diffusive transport took place within the droplets. In addition, the volume fraction of each compartment can be easily controlled. Meanwhile, by adjusting the flow conditions, we varied the sizes of the obtained Janus hydrogel particles ranging from 148 μm to 179 μm with coefficient of variation (CV) value below 5%; their shapes were highly spherical with average roundness over 0.90. In addition, we demonstrated the magnetic and fluorescent performances of the obtained Janus particles. Owing to biocompatibility of the μFEEG method, the device could also prepare cell-laden magnetic Janus hydrogel particles with good cell viability.

II. MATERIALS AND METHODS

A. Microfluidic chip

We designed a microfluidic device consisting of a Janus droplet generator³ located upstream and downstream channels for emulsion-based external gelation³⁷. The Janus Na-alginate droplets, carrying magnetic and/or fluorescent nanoparticles in separate segments, are supposed to form one-by-one in a symmetrically coflowing stream of corn oil; these Janus droplets then react with a fine water-in-oil emulsion containing Ca^{2+} in the downstream channel, forming Janus hydrogel microparticles (**Fig. 1**). The width of the channels was designed to be 200 μm , except for the drain channel, which was set to 400 μm . The depths of upstream and downstream channels were designed to be 200 μm and 400 μm , respectively. The shape of the cross sections is assumed to be rectangular. Through-holes with a diameter of 1.0 mm were designed to connect the microchannels to the outer tubes (**Fig. S1a**).

Channels and through-holes (**Fig. S1b**) were fabricated by computer numerical control (CNC) machining (LB2000 EXII, OKUMA, Japan) equipped with mounted wheels (AAR72, AAR07 AND AAR29, FSK, Japan) on a planar piece of synthetic quartz glass ($15 \times 15 \text{ mm}^2$; thickness: 2 mm). The

microgrooves were sealed with another quartz glass chip of the same size using glass fusion bonding (**Fig. S1c**). Furthermore, to produce water-in-oil (W/O) droplets, the microchannels were subjected to hydrophobic surface modification according to our published protocol³⁷.

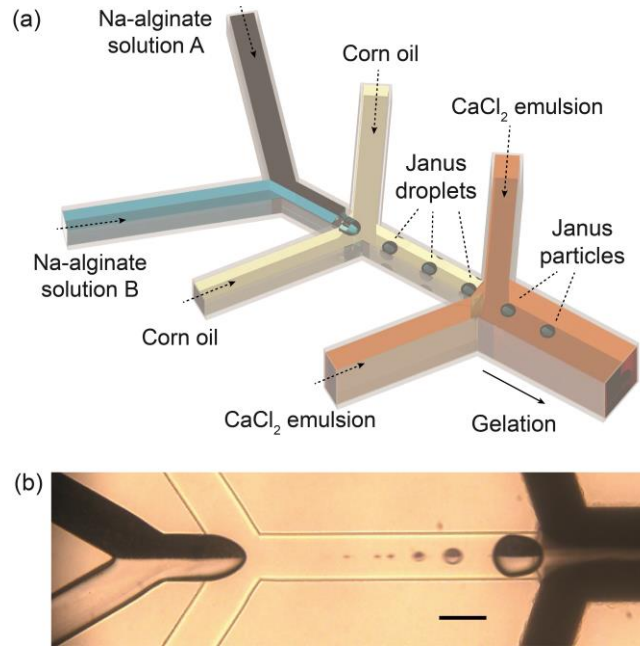


FIG. 1 Microfluidic emulsion-based external gelation (μ FEEG) to produce Janus calcium alginate (Ca-alginate) hydrogel microparticles. (a) A schematic illustration showing the formation of aqueous sodium alginate (Na-alginate) droplets having Janus geometry and their ionic crosslinking by μ FEEG. (b) A snapshot of the generation process of a Janus Na-alginate droplet with magnetic anisotropy. Flow rates of the dispersed phase (Q_d) and continuous phase (Q_c) were 0.1 mL/h (= 0.05 mL/h \times 2) and 2.0 mL/h (= 1.0 mL/h \times 2) respectively. Scale bar is 200 μ m.

B. Materials

The chemicals were purchased from Fujifilm Wako Pure Chemical Corporation (Japan). The Na-alginate powder (80–120 cP, 10 g/L, 20 °C) was dissolved in deionized water (Direct-Q 3UV, 18.2 M Ω , Merck Millipore, USA) at 3 wt% as the pure dispersed phase. Black iron oxide (>95%, Fe₃O₄) nanoparticles were mixed with the aqueous Na-alginate solution at 2 wt% using a disperser (T10 basic

Ultra-Turrax, IKA, Germany) as the magnetic dispersed phase. Fluorescent carboxylate microspheres (excitation wavelength of 441 nm, emission wavelength of 486 nm, 24051-10, 300 nm, Polysciences, USA) were manually dispersed in an aqueous Na-alginate solution at 0.05 wt% as a fluorescent dispersed phase. The details of the dispersed phases are listed in **Table S2**. Corn oil was used as a continuous phase. CaCl₂ powder (>95%) was dissolved in deionized water (30 wt%) as an aqueous solution in the CaCl₂ emulsion. We mechanically mixed the prepared CaCl₂ aqueous solution with corn oil containing a surfactant (SY-Glyster CRS-75, Sakamoto Yakuhin Kogyo Corporation, Japan) at 0.1 wt% by a disperser at 30000 rpm for 3 min; the average diameter of the produced emulsion droplets was 2.2 μm³⁷ (**Fig. S2**). The mass percentage of the aqueous solution (15 g) in this mixture (57 g) was set to 26 wt%, and the average diameter of the prepared CaCl₂ emulsion was 2.2 μm³⁷. This emulsion was infused into the microfluidic device at 15.0 mL/h (= 7.5 mL/h × 2) in all experiments. A 5 wt% aqueous solution of ethylenediaminetetraacetic acid (>99.5%, EDTA, Dojindo, Japan) was used to dissolve the possible clogs in the microchannel caused by accidental gelation.

C. Generation and collection of Janus Ca-alginate microparticles

The fabricated glass microfluidic chip was assembled with a stainless-steel supporting holder that was linked to air-tight glass syringes (1 mL type for dispersed phase, 10 mL type for continuous and reactant phase, 1000 series, Hamilton, USA) carrying prepared solutions by polytetrafluoroethylene (PTFE) tubes (inner diameter: 0.5 mm, outer diameter: 1.59 mm). Dual syringe infusion pumps (KDS 200 and Legato 200, KD Scientific, USA) were used to inject the liquids into the channels. A PTFE tube (inner diameter: 0.8 mm, outer diameter: 1.59 mm) with a length of ~30 cm was used for drainage. We first collected the Janus hydrogel particles in a glass reservoir and then used a nylon mesh (mesh size: 108 μm, Nippon Tokushu Fabric, Japan) to filter the acquired gel beads from the reactant emulsion and undesired satellite particles (average diameter ~50 μm). Hexane (>95%) and deionized water were added to wash out the CaCl₂ emulsion.

The on-chip flow conditions were monitored using a high-speed digital camera (Fastcam Mini AX50, Photron, Japan) mounted on an upright microscope (BX-51, Olympus, Japan). For fluorescent observation, a wide-range excitation fluorescence filter cube (U-MWBV2, Olympus, Japan) was attached to the microscope.

D. Characterization of obtained Janus Na-alginate droplets and Ca-alginate particles

To characterize the Janus droplets, we collected the prepared Janus Na-alginate droplets without gelation in a Petri dish filled with corn oil containing surfactant (SY-Glyster CRS-75) at 5 wt%. For the Janus particles after gelation, we dispersed and observed them in a plastic Petri dish filled with pure water. A digital camera (EOS 60D, Canon, Japan) was used to capture bright-field and fluorescent images of the Janus droplets and particles. ImageJ software (NIH, USA) was used to analyze the diameter D and roundness R of the obtained Janus droplets and hydrogel particles according to the equation below:

$$D = 2 \sqrt{\frac{S}{\pi}} \quad (1)$$

$$R = \frac{4\pi S}{L^2} \quad (2)$$

where S is the projected area, and L is the perimeter of the Janus droplets and microparticles gauged from the microscopic image. We evaluated over 100 samples for each average and CV value of the droplets and hydrogel microparticles. The Janus hydrogel particles were dried for one day at room temperature (~ 23 °C) and observed using a scanning electron microscope (SEM, JSM-6610LA, JEOL, Japan). A neodymium magnet (NK115, 26magnet, Japan) was used to manipulate the magnetic Janus hydrogel beads.

E. Cell encapsulation

HEK-293 cells, which are hypotriploid human cell lines derived from embryonic kidney, were

purchased from Riken BRC, Ibaraki, Japan (RCB1637). The cells were cultured in growth media and incubated at 37 °C in 5% CO₂. The size of these cells was in the range from 11 to 15 μm. The culture medium was Dulbecco's modified Eagle's medium (DMEM) containing 10% (v/v) fetal bovine serum (FBS, Gibco, Thermo Fisher Scientific, USA) and 1% (v/v) penicillin-streptomycin. The cells were detached from the tissue culture flask (Nunc, 75 cm², Thermo Fisher Scientific, USA) by adding 0.25% (w/v) trypsin-ethylenediaminetetraacetic acid (trypsin-EDTA). We labeled the living cells with a fluorescent dye (calcein-AM, excitation/emission wavelength: 490/515 nm, Dojindo, Japan) to evaluate how our particle production process affected their viability.

For cell encapsulation, we added 1 mL of phosphate-buffered saline (PBS) containing cells (concentration: 2.5×10^6 cells/mL), 0.3 g of Na-alginate powder and 0.825 mL of sodium chloride solution (>97%, NaCl, 2 M) to deionized water to adjust the final concentration of Na-alginate at 3wt%. The prepared Na-alginate solution was used as one of the two dispersed phases, and the other dispersed phase was a 3 wt% Na-alginate aqueous solution containing Fe₃O₄ nanoparticles (2 wt%).

Hexadecane (>97%) and deionized water were added alternately to prevent damage to cells during the filtration of cell-laden gel beads³⁸. The obtained cell-laden Ca-alginate particles were collected in a Petri dish with PBS solution for observation.

III. RESULTS AND DISCUSSION

A. Preparation of magnetic Janus Na-alginate droplets

The formation process of magnetic Janus aqueous droplets at the first sheath-flowing junction was initially investigated by infusing pure and magnetic dispersed phases from two upstream inputs (**Fig. 1a**). We set the flow rate of both the pure dispersed phase (Q_{dp}) and magnetic dispersed phase (Q_{dm}) at 0.05 mL/h and continuous phase (Q_c) at 2.0 mL/h (= 1.0 mL/h × 2, **Fig. 1b and S3**). The two input streams of aqueous Na-alginate solutions formed a bicolor laminar flow with a clear boundary at the

center of the channel before reaching the first sheath-flowing junction. Then, magnetic Janus Na-alginate droplets, containing Fe_3O_4 nanoparticles in one hemisphere, could be reproducibly generated at a production rate of ~ 6 drops/s. Together with the main Janus droplet with a diameter of $\sim 224 \mu\text{m}$, the formation of a satellite droplet with a diameter of $\sim 80 \mu\text{m}$ and several smaller satellite droplets was observed because of the high viscosity of the Na-alginate phase ($\sim 1500 \text{ mPa}\cdot\text{s}$). Furthermore, the size of the magnetic segment could be tuned by adjusting the ratio of flow rate between the two disperse phases at a fixed flow rate of the disperse phase ($Q_d = 0.1 \text{ mL/h}$, **Fig. S4**).

The obtained droplets showed clear separation of the two compartments, regardless of whether the values of Q_{dp} and Q_{dm} were the same. We suppose that is because both the diffusive and convective mixing that occurred during the droplet formation and inside the Janus droplets were small. For the diffusion of spherical particles through a liquid with a low *Reynolds* number (ca. 0.02), the mass diffusivity (D) can be defined by a special form of *Stokes-Einstein* equation ³⁹:

$$D = \frac{k_B T}{6\pi\eta r} \quad (3)$$

where k_B is the Boltzmann constant ($1.38 \times 10^{-23} \text{ J/K}$), T represents the thermodynamic temperature (297 K), η is the dynamic viscosity ($1.5 \text{ Pa}\cdot\text{s}$), and r is the radius of the dispersing microspheres ($\sim 150 \text{ nm}$). Based on the equation above, the diffusivity in this case is $9.7 \times 10^{-16} \text{ m}^2/\text{s}$. The average diffusion length inside the Janus Na-alginate droplets can be calculated as:

$$s = \sqrt{2Dt} \quad (4)$$

where t is the time for a droplet to flow out of the drain tube when Q_e was 15 mL/h (30 s). Therefore, the average diffusion length inside the Janus Na-alginate droplet was $2.4 \times 10^{-7} \text{ m}$, suggesting that the diffusive transport inside the Janus droplets was negligible. In convective mixing, the flow tends to recirculate separately in each distinct segment instead of convective transport across the two segments under symmetrical flow condition ³. In addition, we suppose that the high viscosity of the dispersed phase largely decreases the speed of the recirculation flow. As a result, the droplets maintained a strict

Janus structure even when Q_{dp} and Q_{dm} were different.

Monodisperse Na-alginate Janus droplets of varying diameters and a CV value below 4% were prepared when we tuned Q_c from 1.0 to 3.0 mL/h and a fixed Q_d of 0.1 mL/h (**Fig. 2a**). The diameter of the Janus droplets gradually decreased as Q_c increased. We obtained Janus droplets with an average diameter of around 224 μm (CV value: 2.3%) when Q_c was 1.0 mL/h (**Fig. 2b-A**). The average diameter reduced slightly to 202 μm (CV value: 3.2%) when Q_c increased to 2.0 mL/h (**Fig. 2b-B**). However, when Q_c was increased further, the produced droplets did not decrease in size. When Q_c was as high as 3.0 mL/h, the average diameter of the formed Janus droplets was 202 μm with a CV of 3.8% (**Fig. 2b-C**). We consider that this plateau in droplet size at higher Q_c is due to the transition of droplet formation from dripping to jetting regime⁴⁰ (**Fig. S5**). We also prepared a phase diagram showing the conditions under which Janus Na-alginate droplets could form (**Fig. S6**).

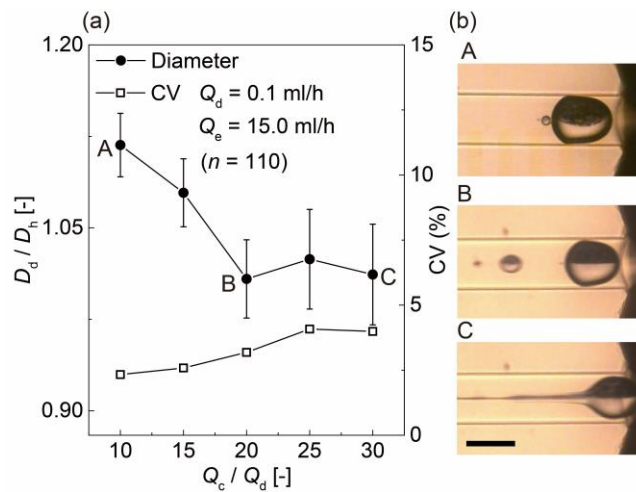


FIG. 2 Influence of Q_c on the diameters of obtained Janus droplet. (a) The Q_c / Q_d vs. the diameter and its coefficient of variation (CV) of the produced Janus droplets. D_d represents the diameter of Janus droplet. D_h is the hydraulic diameter of the orifice, which is $D_h = 4 A P^{-1}$, where A and P are the cross-section area and perimeter of the orifice respectively. (b) Microscopic images of generation process of Janus droplets in the microchannel at (A) $Q_c / Q_d = 10.0$, (B) $Q_c / Q_d = 20.0$, (C) $Q_c / Q_d = 30.0$. $Q_d = 0.1$ mL/h (= 0.05 mL/h \times 2). Scale bar is 200 μm .

B. Preparation and characterization of magnetic Janus Ca-alginate microparticles

The generated Janus droplets reacted with the emulsion co-flow at the second sheath-flowing junction (**Fig. 1a**). After filtration with deionized water, we obtained monodisperse magnetic Janus gel particles with a diameter of 148 μm and a CV of 3.7% ($n = 188$) when the Q_d , Q_c and Q_e were set to 0.1 mL/h, 2.0 mL/h and 15.0 mL/h, respectively (**Fig. 3a and 3b**). Compared to the Janus droplets generated at the same Q_c/Q_d values, the diameters of the obtained Janus hydrogel particles decreased after gelation. The shrinkage of gel beads was probably caused by the cross-linking reaction, in which the calcium ions connect and close the alginate molecules⁴¹. The produced gel particles had an average roundness of 0.96, and 99% of the particles had roundness over 0.90, indicating that the majority of hydrogel particles were highly spherical (**Fig. 3c**). The Janus structure of the hydrogel particles we produced was stable in pure water for a month (**Fig. S7**), suggesting that the Fe_3O_4 nanoparticles were firmly entrapped and immobilized by the alginate polymer network. This result is in accordance with previous research, where the mesh size of a Ca-alginate cross-linking network structure was mostly below 30 nm⁴². The SEM images obtained at higher magnifications also suggests that the mesh size of the crosslinked alginate network is below 30 nm (**Fig. S8**). As a result, the magnetic particles (~ 500 nm), which were much larger than the mesh sizes of the alginate polymeric network, could not move and disperse after the gelation process was completed.

Besides, monodisperse spherical magnetic Janus hydrogel particles of varying sizes could be prepared by simply adjusting Q_c and maintaining a fixed Q_d ($0.05 \text{ mL/h} \times 2$) and Q_e (15.0 mL/h). **Figure 3d** shows the relationship between the Q_c/Q_d values and diameters and the deviations of the prepared Janus Ca-alginate gel particles. Based on the experimental results, we confirmed that the size of Janus hydrogel particles could be easily manipulated by varying the Q_c/Q_d values from 10.0% to 20.0%. Thus, we prepared monodisperse gel beads with diameters ranging from 148 μm to 179 μm . The narrow size distributions of the prepared hydrogel beads (CV values $< 5\%$) indicate high

monodispersity. The bright-field images of the magnetic Janus hydrogel particles with diameters of approximately $179 \mu\text{m}$ (**Fig. 3d-I**) and $148 \mu\text{m}$ (**Fig. 3d-II**) show that the generated Janus gel beads had very clear boundaries between the magnetic and non-magnetic segments.

Furthermore, the volume fraction of the magnetic compartment in the Janus hydrogel particles was strictly regulated by simply adjusting the flow rate ratio of the magnetic dispersed phase (Q_{dm}) to the total dispersed phase (**Fig. S4**). We prepared magnetic Janus microgel particles with a volume fraction of the magnetic compartment at 0.25 (**Fig. 3e-A**), 0.50 (**Fig. 3e-B**), and 0.75 (**Fig. 3e-C**). The experimental results show the possibility of synthesizing Janus hydrogel particles with well-defined interfaces and different volume proportions between the two compartments.

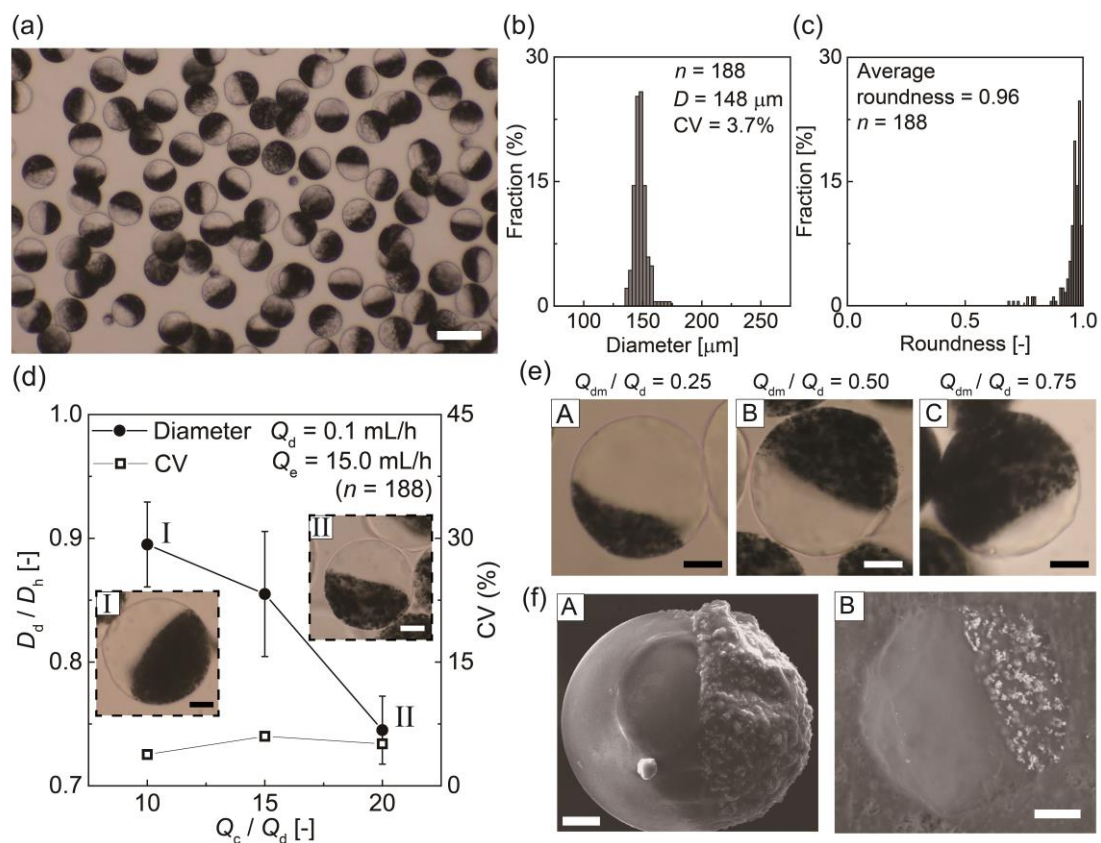


FIG. 3 Magnetic Janus hydrogel microparticles prepared by μ FEEG. $Q_e = 15.0 \text{ mL/h}$. (a-c) Obtained Janus microparticles in pure water at $Q_c / Q_d = 20.0$, $Q_d = 0.1 \text{ mL/h}$ ($= 0.05 \text{ mL/h} \times 2$): (a) Micrograph of obtained gel beads in pure water (Scale bar: $200 \mu\text{m}$). (b) Distribution graph of size of hydrogel

particles. (c) Roundness distribution of hydrogel particles. (d) Flow rate ratio between the Q_c / Q_d vs. the diameters and CVs of Janus hydrogel particles. Scale bars are 40 μm . (e) Hydrogel particles prepared at different flow rate ratios of magnetic dispersed phase (Q_{dm}) to total dispersed phase (Q_d): (A) $Q_{dm} / Q_d = 0.25$, (B) $Q_{dm} / Q_d = 0.50$ and (C) $Q_{dm} / Q_d = 0.75$. $Q_d = 0.1 \text{ mL/h}$, $Q_c = 2.0 \text{ mL/h}$. Scale bars are 40 μm . (f) SEM images of an aerogel bead showing: (A) surface of Fe_3O_4 structure (Scale bar: 30 μm) and (B) cross-section view (Scale bar: 20 μm).

The clear interface between the two segments of the produced Janus hydrogel beads proves that the gelation speed of the Janus droplets downstream is high. The rapid gelation reaction eliminated the possible convective and diffusive transport inside the droplets. We suppose that gelation would be completed in the drain tube, where the residence time of the droplets/particles was $\sim 30 \text{ s}$. We consider that this attributed to the sufficient concentration of Ca^{2+} in the CaCl_2 emulsion phase (0.675 mol/L).

To investigate the internal Janus structure of the obtained hydrogel beads further, we dried the magnetic Janus hydrogel particles for SEM observation. We confirmed that the dried Janus aerogel particles could maintain a spherical shape with a smooth hemisphere and the other hemisphere was a rough surface with Fe_3O_4 nanoparticles (**Fig. 3f-A and S9**). No significant shrinkage of the gels was observed after drying. The SEM image of their cross-sections showed that the Fe_3O_4 nanoparticles existed only on one side of the microparticles (**Fig. 3f-B**). Based on the SEM images, we could strictly define the boundary between the magnetic and non-magnetic segments, proving that our Ca-alginate particles had an obvious Janus morphology.

C. Magnetic Janus Ca-alginate microparticles with fluorescent anisotropy

First, Janus Ca-alginate microparticles with only fluorescent anisotropy were prepared by hemispheric encapsulation of the fluorescent nanoparticles in microgel beads. We prepared the fluorescent Janus gel particles by infusing the fluorescent and pure dispersed phases to the upstream sheath-flowing junction at the same flow rate (0.05 mL/h, **Fig. S10**). The obtained Janus microspheres

showed bi-compartmental structures in both bright-field and fluorescence microscopy (**Fig. S11**). The fluorescent Janus hydrogel particles we produced presented clear interfaces between their compartments (**Fig. S12**).

We then produced Janus Ca-alginate gel beads with both magnetic and fluorescent anisotropy by equally infusing the fluorescent and magnetic dispersed phase into the sheath-flowing junction ($0.05 \text{ mL/h} \times 2$). The production rate of Janus droplets was ~ 6 drops/s when the same flow rates ($Q_d = 0.1 \text{ mL/h}$, $Q_c = 2.0 \text{ mL/h}$) were set (**Fig. S13**). The similar production rate (~ 6 drops/s) suggests that the incorporation of nanoparticles (Fe_3O_4 and fluorescent nanoparticles) had no significant effect on the process of droplet formation.

Janus particles loaded hemispherically with Fe_3O_4 nanoparticles are shown in the bright-field images. Meanwhile, the fluorescence of the other segment of the Janus beads was confirmed using a fluorescence microscope (**Fig. 4a**). The boundary between the bi-color segments was clear and two hemispherical segments could be clearly distinguished. The average diameter of the obtained Janus beads was $150 \mu\text{m}$ (CV value: 4.0%), and they were highly spherical in shape with an average roundness of 0.97 (**Fig. 4b and 4c**). From the SEM image of a dried magnetic-fluorescent Janus aerogel bead, we confirmed that the obtained Janus microbeads had one hemispherical surface filled with Fe_3O_4 nanoparticles (**Fig. 4d**). From the SEM image in Fig. 3f, we consider that the hemisphere of this Janus particle was also filled with Fe_3O_4 nanoparticles similarly. However, the fluorescent nanoparticles on the other half of the surface were not observed, which could have been caused by the low volume fraction of fluorescent particles in the original Na-alginate solution ($6 \times 10^{-5} \text{ v/v\%}$) compared to the magnetic nanoparticles (ca. 0.38 v/v%).

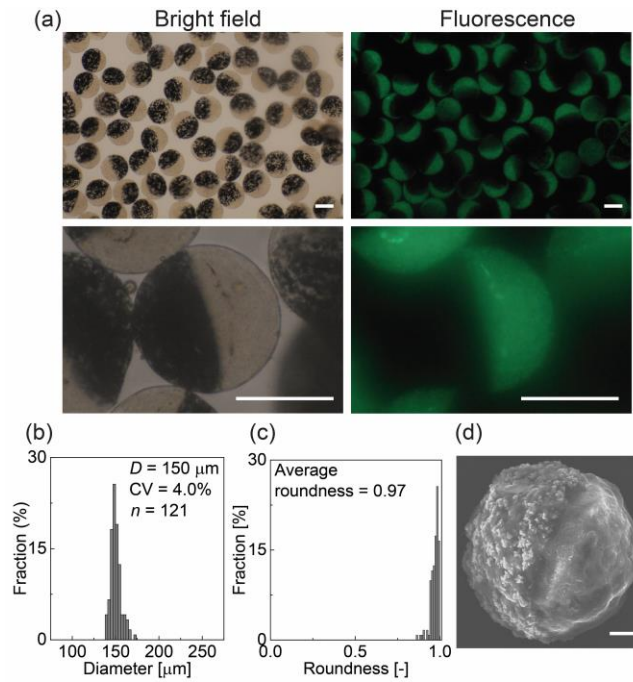


FIG. 4 Janus Ca-alginate hydrogel particles with both magnetic and fluorescent anisotropy. (a) Janus hydrogel particles observed by bright-field and fluorescent microscopy in pure water. Scale bars are 100 μm . (b) Distribution graph of particles' size. (c) Roundness distribution of hydrogel particles. (d) A SEM photo of a dried magnetic-fluorescent Janus microparticle. Scale bar is 10 μm .

D. Encapsulation of mammalian cell

To examine biocompatibility of our μFEEG method, we encapsulated viable mammalian cells in one hemisphere of the magnetic Janus hydrogel microspheres. We prepared the magnetic Janus gel particles that encapsulate cells by equally infusing magnetic dispersed phase and dispersed phases containing cells to the upstream sheath-flowing junction (**Fig. S14**). The obtained magnetic Janus hydrogel particles showed that the cells were separately co-encapsulated with Fe_3O_4 particles, while most Janus beads maintained a highly spherical shape (**Fig. 5a**). We calculated the calcein-AM-labeled living cells before and after their encapsulation inside the Janus microspheres (**Fig. 5b**) and found that the viability of the cells slightly decreased from 89% ($n = 267$) to 85% ($n = 158$) via particle production.

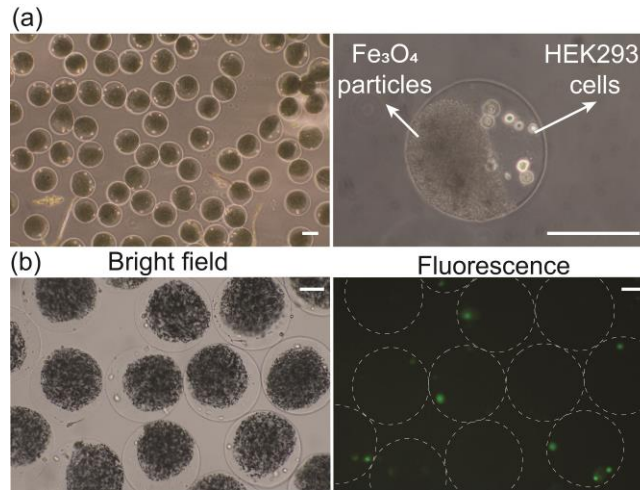


FIG. 5 Janus Ca-alginate hydrogel particles encapsulating human cells (HEK-293). (a) Janus hydrogel particles encapsulating HEK-293 cells observed by bright-field at different magnifications. Scale bars are 100 μm . (b) Bright-field and fluorescent microscopy images of Janus hydrogel particles encapsulating stained HEK-293 cells. Scale bars are 50 μm .

The viability of encapsulated cells proves that our μFEEG method is biocompatible, based on previous studies on cell-laden alginate microparticles^{16,38}. The corn oil phase and hexadecane used in filtration did not cause significant cytotoxicity to the embedded cells. The incorporation of magnetic particles and mammalian cells separately in the two segments of a single Janus microsphere has great potential in biological experiments. A promising application might be in the functional tissue construction¹⁵ because such Janus particles can be magnetically manipulated and assembled into the ordered patterns while they allow a clear view of the culturing cells. Targeted delivery of stem cells for cartilage repair⁴³ might be another promising application.

E. Magnetic manipulations of Janus Ca-alginate microparticles

To examine the magnetic functionality of Janus Ca-alginate microparticles produced by us, magnetic field (20 mT, in-plane) was applied across the particles in a Petri dish with the help of two magnets facing each other. Similar to previous reports on magnetic Janus microparticles^{15,17,33}, the magnetic

Janus hydrogel particles could self-assemble into a single (**Fig. 6a-A**) and double (**Fig. 6a-B**) pearl-chain structures in response to the parallel magnetic field. The magnetic Janus beads formed a mesh-like structure as parallel chains zippered together when the concentration of the particles in the observation reservoir was high (**Fig. 6a-C**)¹⁷. **Figure 6b** shows the self-assembly of magnetic-fluorescent Janus hydrogel particles. In addition, **Fig. 6c** shows optical images of a Janus hydrogel particle rotating in an externally applied magnetic field. The results show that under a manually applied rotational magnetic field, the resulting torque drove the Janus hydrogel particles to rotate clockwise in a well-controlled manner. We also demonstrated the actuation of magnetic-fluorescent Janus Calcium alginate gel particles by applying a magnet on one side of the collected particles. The Janus beads with fluorescence were quickly pulled towards the wall and effectively accumulated by using a neodymium magnet (**Fig. 6d**).

The results of magnetic manipulations proved that the bifunctional hydrogel microspheres that we produced had strong fluorescence and excellent magnetism. Such magnetic functionality will be particularly useful for applications such as the preparation of magneto-rheological fluids¹¹, micro-mixing, and micro-sorting¹⁷.

Unlike the previous microfluidic systems for generating similar Janus hydrogel microparticles, our fabrication system does not need the precise flow-rate control for droplet-droplet coalescence and the process to disperse Ca²⁺ ions in the oil phase. Meanwhile, we believe that this work can be improved further in the following aspects. Firstly, the production rate of hydrogel particles (~ 6 particles s⁻¹) in this study is limited to a single microfluidic droplet generator; we envision scaled-up production via parallelization of many channels on a chip¹, which will be useful for practical industrial applications. Secondly, an on-chip approach for synthesizing CaCl₂ emulsion could maintain stability of the reactant emulsion and achieve production of hydrogel particles over a long duration. Thirdly, smaller-sized hydrogel particles (e.g., 50 μm in diameter) will be prepared by simply reducing the dimensions of the microchannels and preparing CaCl₂ emulsions of appropriate sizes. Decreasing the Na-alginate

concentration and the viscosity of the solution will also assist the production of smaller particles at higher frequency. For example, 0.5 wt% alginate solution was used to make a cross-linked alginate film with the pore size range of 6.0-16 nm previously⁴⁴. Meanwhile, we consider that a higher alginate concentration will make mechanically and physically more superior hydrogel particles because of the increased polymer network density.

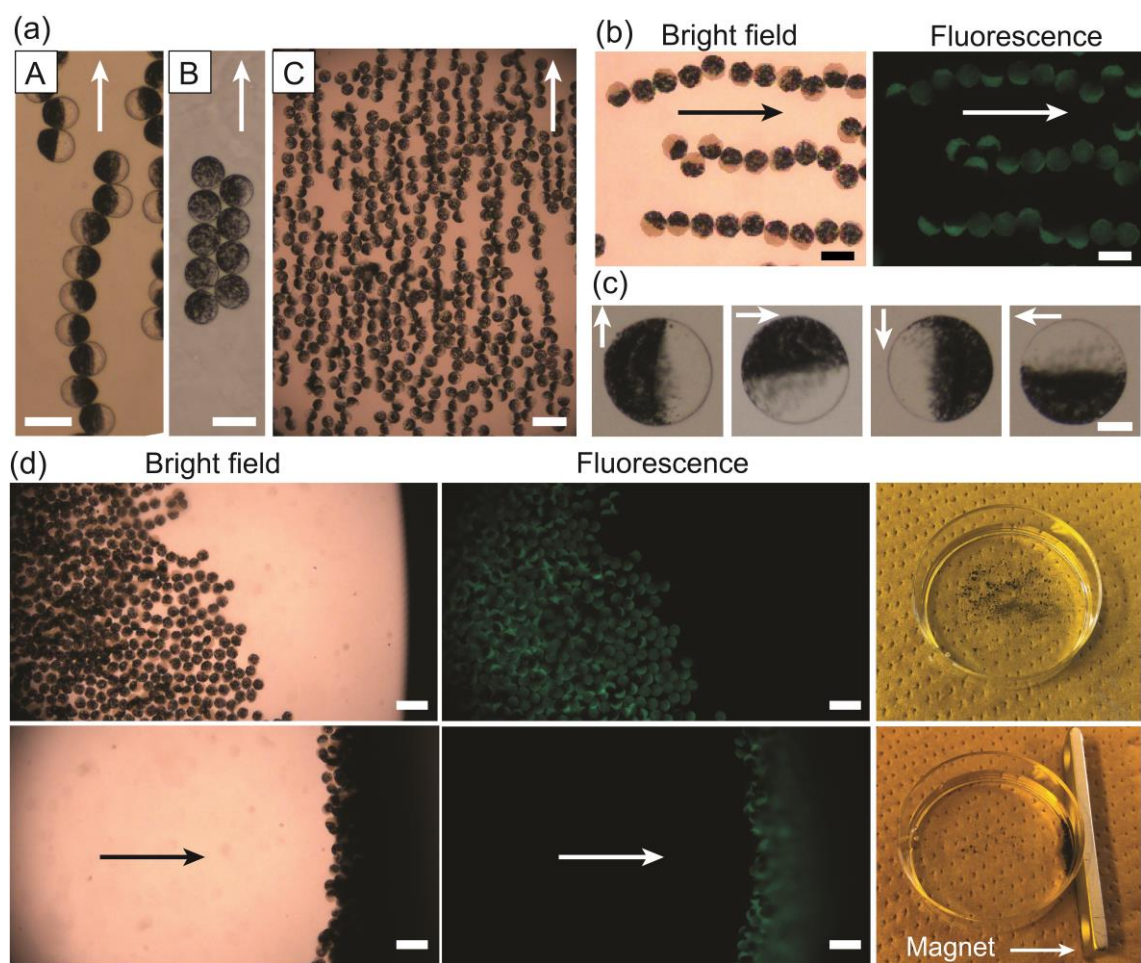


FIG. 6 Magnetic Janus hydrogel particles in response to the magnetic field. The arrows indicate the orientation of the magnetic field. (a) Self-assembling Janus hydrogel particles in a (A) single, (B) double chainlike structures (Scale bar: 200 μm) and (C) self-assembling Janus gels at high particle concentration (Scale bar: 400 μm). (b) Self-assembling Janus hydrogel particles with both magnetic and fluorescent anisotropy (Scale bar: 200 μm). (c) Microscopic photos of a Janus hydrogel particle

spinning in a rotating magnetic field (Scale bar: 50 μm). (d) Micrographs of the magnetically actuated Janus hydrogel in water before and after the application of a magnetic field. Scale bars are 400 μm .

In addition to the magneto-responsive Janus microparticles, our strategy offers an approach for preparing hydrogel microparticles with other prospects. First, the roughness-anisotropic surface of our gel microparticles shows the possibility of fabrication of colloid beads with site-specific roughness on their surface, which might be useful as a substance for bio-tissue engineering^{45,46}. Second, this approach is also potentially suitable for the fabrication of “patchy particles”⁴⁷: particles with dual or multiple patches of diverse properties, which could be highly used in photonics, sensors, and electronics applications. Thirdly, a strictly defined Janus structure of monodisperse beads with demanding functions could be achieved by encapsulating different materials in a separate segment, which might have great potential in diverse biological applications.

IV. CONCLUSION

We demonstrated for the first time that microfluidic emulsion-based external gelation (μFEEG) can be applied for the synthesis of Janus Ca-alginate hydrogel microparticles. Monodisperse and highly spherical Janus Ca-alginate beads with magnetic anisotropy were fabricated with average diameters ranging from 148 to 179 μm , CV values below 4%, and roundness >0.93 . These Janus beads had a clear boundary between the two segments with tunable volume fractions. Fluorescent anisotropy can also be applied to hydrogel particles through the incorporation of fluorescent nanoparticles into the segments. Mammalian cell-laden magnetic Janus hydrogel particles could be prepared because of biocompatibility of the FEEG method. Finally, magnetic manipulation of the Janus hydrogel microparticles was demonstrated. We believe that the present approach is promising for preparing monodisperse Janus hydrogel microbeads of similar biopolymers, suitable for use in numerous applications including glucose sensing⁴⁸ and DNA assay detection¹⁷.

SUPPLEMENTARY MATERIAL

See supplementary material for the microfluidic chip, the emulsion size distribution, the photomicrographs of the Janus droplet generation and hydrogel particles, the SEM images of the alginate, and Tables of the microfluidic methods in literature and experimental conditions.

ACKNOWLEDGMENTS

This work was supported by JSPS KAKENHI Grant Numbers 16K04916, 20H02512.

AUTHOR DECLARATIONS

Conflict of Interest

The authors have no conflicts to disclose.

REFERENCES

1. T. Nisisako, "Recent advances in microfluidic production of Janus droplets and particles," *Curr. Opin. Colloid Interface Sci.* **25**, 1–12 (2016). <https://doi.org/10.1016/j.cocis.2016.05.003>.
2. S. Lone, I.W. Cheong, "Fabrication of polymeric Janus particles by droplet microfluidics," *RSC Adv.* **4**, 13322–13333 (2014). <https://doi.org/10.1039/c4ra00158c>.
3. T. Nisisako, T. Torii, T. Takahashi, Y. Takizawa, "Synthesis of monodisperse bicolored Janus particles with electrical anisotropy using a microfluidic co-flow system," *Adv. Mater.* **18**, 1152–1156 (2006). <https://doi.org/10.1002/adma.200502431>.
4. C. C asagramde, P. Fabre, E. Raphael, M. Veyssie, "Janus beads: Realization and behaviour at water/oil interfaces," *Europhys. Lett.* **9**, 251–255 (1989). <https://doi.org/10.1209/0295-5075/9/3/011>.
5. S. Berger, A. Synytska, L. Ionov, K.J. Eichhorn, M. Stamm, "Stimuli-responsice bicomponent

- polymer Janus particles by ‘Grafting from’/‘Grafting’ to approaches,” *Macromolecules* **41**, 9669–9676 (2008). <https://doi.org/10.1021/ma802089h>.
6. Y. Du, E. Lo, S. Ali, A. Khademhosseini, “Direct assembly of cell-laden microgels for fabrication of 3D tissue constructs,” *PNAS* **105**, 9522–9527 (2008). <https://doi.org/10.1073/pnas.0801866105>.
 7. W.F. Lai, A.S. Susha, A.L. Rogach, “Multicompartment microgel beads for co-delivery of multiple drugs at individual release rates,” *ACS Appl. Mater. Interfaces* **8**, 871–880 (2016). <https://doi.org/10.1021/acsami.5b10274>.
 8. V. Rastogi, S. Melle, O.G. Calderon, A.A. Garcia, M. Marquez, O.D. Velev, “Synthesis of light-diffracting assemblies from microspheres and nanoparticles in droplets on a superhydrophobic surface,” *Adv. Mater.* **20**, 4263–4268 (2008). <https://doi.org/10.1002/adma.200703008>.
 9. Y. Komazaki, H. Hiramata, T. Torii, “Electrically and magnetically dual-driven Janus particles for handwriting-enabled electronic paper,” *J. Appl. Phys.* **117**, 154506 (2015). <https://doi.org/10.1063/1.4917379>.
 10. J.N. Anker, C. Behrend, R. Kopelman, “Aspherical magnetically modulated optical nanoprobe (MagMOONs),” *J. Appl. Phys.* **93**, 6698–6700 (2003). <https://doi.org/10.1063/1.1556926>.
 11. B. Ren, A. Ruditskiy, J.H. Song, I. Kretzschmar, “Assembly behavior of iron oxide-capped Janus particles in a magnetic field,” *Langmuir* **28**, 1149–1156 (2012). <https://doi.org/10.1021/la203969f>.
 12. L. Baraban, D. Makarov, R. Streubel, I. Monch, D. Grimm, S. Sanchez, O.G. Schmidt, “Catalytic Janus motors on microfluidic chip: deterministic motion for targeted cargo delivery,” *ACS Nano* **6**, 3383–3389 (2012). <https://doi.org/10.1021/nn300413p>.
 13. L.O. Mair, B. Evans, A.R. Hall, J. Carpenter, A. Shields, K. Ford, M. Millard, R. Superfine, “Highly controllable near-surface swimming of magnetic Janus nanorods: application to payload capture and manipulation,” *J. Phys. D: Appl. Phys.* **44**, 125001 (2011). <https://doi.org/10.1088/0022-3727/44/12/125001>.
 14. H. Wang, S. Yang, S.N. Yin, L. Chen, S. Chen, “Janus suprabead displays derived from the

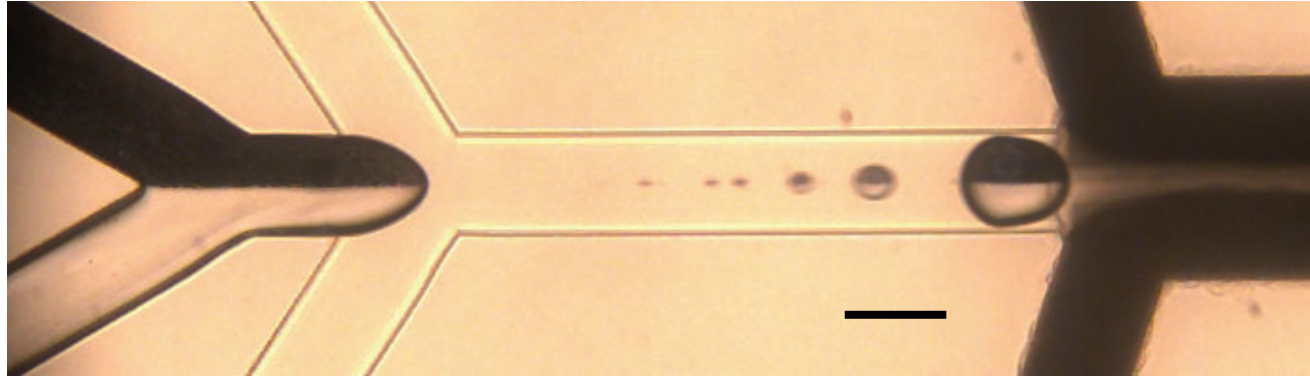
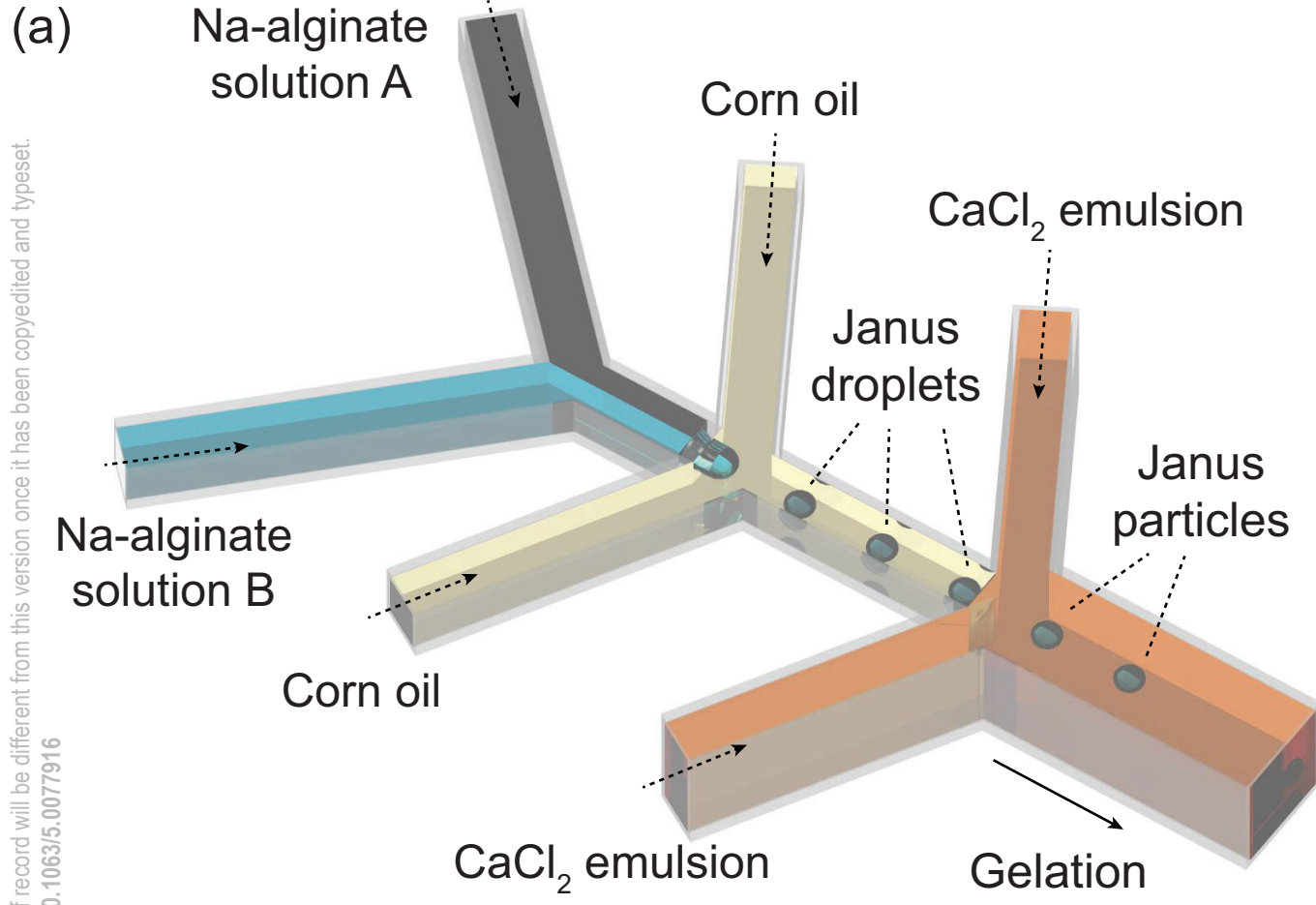
- modified photonic crystals toward temperature magnetism and optics multiple responses,” ACS Appl. Mater. Interfaces **7**, 8827–8833 (2015). <https://doi.org/10.1021/acsami.5b01436>.
15. K. Maeda, H. Onoe, M. Takinoue, S. Takeuchi, “Controlled synthesis of 3D multt-copmpartmental particles with centrifuge-based microdroplet formation from a multi-barrelled capillary,” Adv. Mater. **24**, 1340–1346 (2012). <https://doi.org/10.1002/adma.201102560>.
 16. L.B. Zhao, L. Pan, K. Zhang, S.S. Guo, W. Liu, Y. Wang, Y. Chen, X.Z. Zhao, H.L.W. Chen, “Generation of Janus alginate hydrogel particles with magnetic anisotropy for cell encapsulation,” Lab on chip **9**, 2981–2986 (2009). <https://doi.org/10.1039/b907478c>.
 17. K.P. Yuet, D.K. Hwang, R. Haghgooie, P.S. Doyle, “Multifunctional superparamagnetic Janus particles,” Langmuir **26**, 4281–4287 (2010). <https://doi.org/10.1021/la903348s>.
 18. J. Lan, J.Chen, N. Li, X. Ji, M. Yu, Z. He, “Microfluidic generation of magnetic-fluorescent Janus microparticles for biomolecular detection,” Talanta **151**, 126–131 (2016). <https://doi.org/10.1016/j.talanta.2016.01.024>.
 19. P. Alivisatos, “The use of nanocrystals in biological detection,” Nat. Biotechnol. **22**, 47–52 (2004). <https://doi:10.1038/nbt927>.
 20. V. Stsiapura, A. Sukhanova, M. Artemyev, M. Pluot, J.H.M. Cohen, A.V. Baranov, V. Oleinikov, I. Nabiev, “Functionalized nanocrystal-tagged fluorescent polymer beads: synthesis, physicochemical characterication, and immunolabeling application,” Anal. Biochem. **334**, 257–265 (2004). <https://doi.org/10.1016/j.ab.2004.07.006>.
 21. B.M. Teo, D.J. Young, X.J. Loh, “Magnetic anisotropic particles: toward remotely actuated applications,” Part. Part. Syst. Charact. **33**, 709–728 (2016). <https://doi.org/10.1002/ppsc.201600060>.
 22. C. Xu, B. Wang, S. Sun, “Dumbbell-like Au-Fe₃O₄ nanoparticles for target-specific platin delivery,” J. Am. Chem. Soc. **131**, 4216–4217 (2009). <https://doi.org/10.1021/ja900790v>.
 23. S.H. Hu, X. Gao, “Manocomposites with spatially separated functionalities for combined imaging

- and magnetolytic therapy,” *J. Am. Chem. Soc.* **132**, 7234–7237 (2010).
<https://doi.org/10.1021/ja102489q>.
24. X.Y. Ling, I.Y. Phand, C. Acikgoz, M.D. Yilmaz, M.A. Hempenious, G.J. Vancso, J. Huskens, “Janus particles with controllable patchiness and their chemical functionalization and supramolecular assembly,” *Angew. Chem. Int. Ed.* **48**, 7677–7682 (2009).
<https://doi.org/10.1002/anie.200903579>.
25. Y. Zhang, Y. Wan, Y. Liao, Y. Hu, T. Jiang, T. He, W. Bi, J. Lin, P. Gong, L. Tang, et al., “Janus γ -Fe₂O₃/SiO₂-based nanotheranostics for dual-modal imaging and enhanced synergistic cancer starvation/chemodynamic therapy,” *Science Bulletin* **65**, 564–572 (2020).
<https://doi.org/10.1016/j.scib.2019.12.024>.
26. H. Yabu, M. Kanahara, M. Shimomura, T. Arita, K. Harano, E. Nakamura, T. Higuchi, H. Jinnai, “Polymer Janus particles containing block-copolymer stabilized magnetic nanoparticles,” *ACS Appl. Mater. Interfaces* **5**, 3262–3266 (2013). <https://doi.org/10.1021/am4003149>.
27. K.H. Roh, D.C. Martin, A.J. Lahann, “Biphasic Janus particles with nanoscale anisotropy,” *Nature Mater.* **4**, 759–763 (2005). <https://doi.org/10.1038/nmat1486>.
28. S.N. Yin, C.F. Wang, Z.Y. Yu, J. Wang, S.S. Liu, S. Chen, “Versatile bifunctional magnetic-fluorescent responsive Janus supraballs towards the flexible bead display,” *Adv. Mater.* **23**, 2915–2919 (2011). <https://doi.org/10.1002/adma.201100203>.
29. Y. Zhao, H.C. Shum, H. Chen, L.L.A. Adams, Z. Gu, D.A. Weitz, “Microfluidic generation of multifunctional quantum dot barcode particles,” *J. Am. Chem. Soc.* **133**, 8790–8793 (2011).
<https://doi.org/10.1021/ja200729w>.
30. R.K. Shah, J.W. Kim, D.A. Weitz, “Janus supraparticles by induced phase separation of nanoparticles in droplets,” *Adv. Mater.* **21**, 1949–1953 (2009).
<https://doi.org/10.1002/adma.200803115>.
31. S.H. Kim, J.Y. Sim, J.M. Lim, S.M. Yang, “Magneto-responsive microparticles with nanoscopic

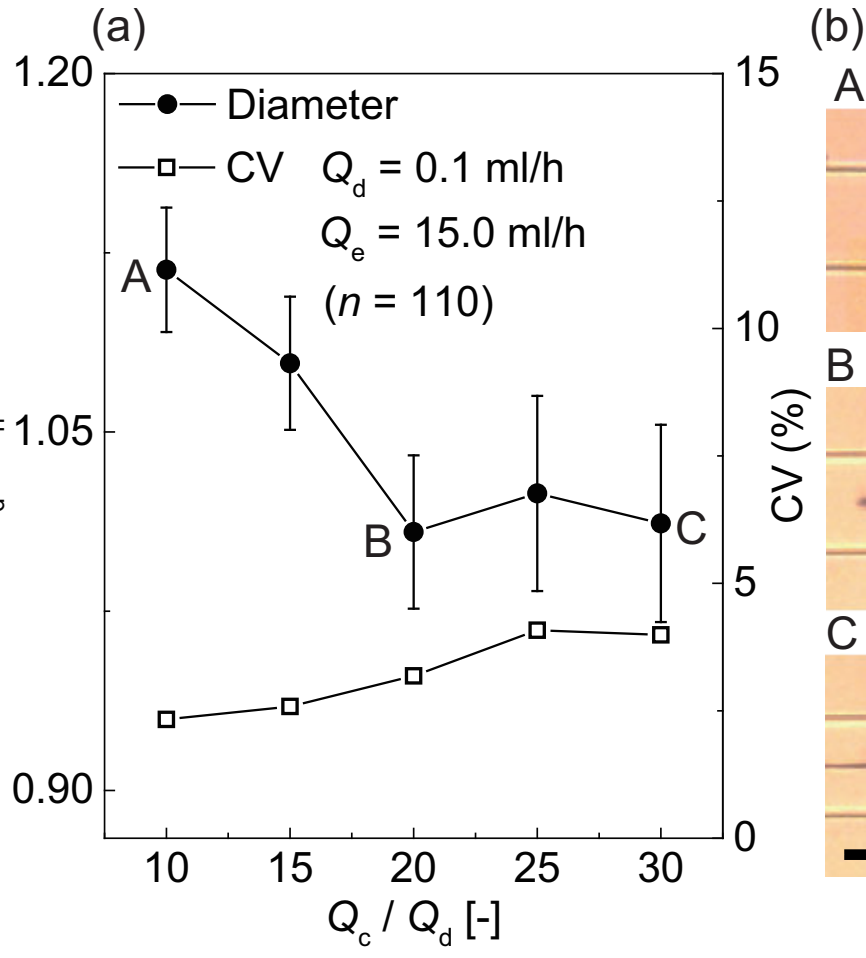
- surface structures for remote-controlled locomotion,” *Angew. Chem.* **49**, 3786–3790 (2010). <https://doi.org/10.1002/anie.201001031>.
32. S. Li, X. Yu, S. You, B. Cai, C. Liu, H. Liu, W. Liu, S.S. Guo, X.Z. Zhao, “Generation of BiFeO₃-Fe₃O₄ Janus particles based on droplet microfluidic method,” *Appl. Phys. Lett.* **105**, 042903 (2014).
33. S. Yoshida, M. Takinoue, E. Iwase, H. Onoe, “Dynamic transformation of self-assembled structures using anisotropic magnetized hydrogel microparticles,” *J. Appl. Phys.* **120**, 084905 (2016). <https://doi.org/10.1063/1.4961422>.
34. P. Aslani, R.A. Kennedy, “Effect of gelation conditions and dissolution media on the release of paracetamol from alginate gel beads,” *J. Microencapsulation* **13**, 601–614 (1996). <https://doi.org/10.3109/02652049609026044>.
35. L. Zhang, K. Chen, H. Zhang, B. Pang, C.H. Choi, A.S. Mao, H. Liao, S. Utech, D.J. Mooney, H. Wang, D.A. Weitz, “Microfluidic templated multicompartment microgels for 3D encapsulation and paring of single cells,” *Small* **14**, 1702955 (2018). <https://doi.org/10.1002/sml.201702955>.
36. Aketagawa, H. Hirama, T. Torii, “Hyper-miniaturisation of monodisperse Janus hydrogel beads with magnetic anisotropy based on coagulation of Fe₃O₄ nanoparticles,” *J. Mater. Sci. Chem. Eng.* **1**, 1–5 (2013). <https://doi.org/10.4236/msce.2013.12001>
37. Y. Liu, N. Tottori, T. Nisisako, “Microfluidic synthesis of highly spherical calcium alginate hydrogels based on external gelation using an emulsion reactant,” *Sensors Actuators, B Chem.* **283**, 802–809 (2019). <https://doi.org/10.1016/j.snb.2018.12.101>.
38. W.H. Tan, S. Takeuchi, “Monodisperse alginate hydrogel microbeads for cell encapsulation,” *Adv. Mater.* **19**, 2696–2701 (2007). <https://doi.org/10.1002/adma.200700433>.
39. A. Einstein, “Investigations on the theory of Brownian movement,” (Dover Publications, New York, 1956).
40. A.S. Utada, E. Lorenceau, D.R. Link, P.D. Kaplan, H.A. Stone, D.A. Weitz, “Monodisperse double emulsions generated from a microcapillary device,” *Science* **308**, 537–541 (2005).

- <https://doi.org/10.1126/science.1109164>.
41. C.K. Kuo, P.X. Ma, “Ionically crosslinked alginate hydrogels as scaffolds for tissue engineering: Part 1. Structure, gelation rate and mechanical properties,” *Biomaterials* **22**, 511–521 (2001).
[https://doi.org/10.1016/s0142-9612\(00\)00201-5](https://doi.org/10.1016/s0142-9612(00)00201-5).
 42. A.W. Chan, R.J. Neufeld, “Tuneable semi-synthetic network alginate for absorptive encapsulation and controlled release of protein therapeutics,” *Biomaterials* **31**, 9040–9047 (2010).
<https://doi.org/10.1016/j.biomaterials.2010.07.111>.
 43. R.G. Thomas, A.R. Unnithan, M.J. Moon, S.P. Surendran, T. Batgerel, C.H. Park, C.S. Kim, Y.Y. Jeong, “Electromagnetic manipulation enabled calcium alginate Janus microsphere for targeted delivery of mesenchymal stem cells,” *Int. J. Biol. Macromol.* **110**, 465–471 (2018).
<https://doi.org/10.1016/j.ijbiomac.2018.01.003>.
 44. C. Simpliciano, L. Clark, B. Asi, N. Chu, M. Mercado, S. Diaz, M. Goedert, M. Mobed-Miremadi, *J. Surf. Eng. Mater. Adv. Technol.* **3**, 1-12 (2013). <http://dx.doi.org/10.4236/jsemat.2013.34A1001>.
 45. L. Ponsonnet, K. Reybier, N. Jaffrezic, V. Comte, C. Lagneau, M. Lissac, C. Martelet, “Relationship between surface properties (roughness, wettability) of titanium and titanium alloys and cell behavior,” *Mater. Sci. Eng. C* **23**, 551–560 (2003). [https://doi.org/10.1016/S0928-4931\(03\)00033-X](https://doi.org/10.1016/S0928-4931(03)00033-X).
 46. N.J. Hallab, K.J. Bundy, K. O’Connor, R.L. Moses, J.J. Jacobs, “Evaluation of metallic and polymeric biomaterials surface energy and surface roughness characteristics for directed cell adhesion,” *Tissue Engineering* **7**, 55–71 (2001). <https://doi.org/10.1089/107632700300003297>.
 47. A.B. Pawar, I. Kretzschmar, “Fabrication, assembly, and application of patchy particles,” *Macromol. Rapid Commun.* **31**, 150–168 (2010). <https://doi.org/10.1002/marc.200900614>.
 48. X.T. Sun, Y. Zhang, D.H. Zhang, S. Yue, C.G. Yang and Z.R. Xu, “Multitarget sensing of glucose and cholesterol based on Janus hydrogel microparticles,” *Biosens. Bioelectron.* **92**, 81–86 (2017).
<https://doi.org/10.1016/j.bios.2017.02.008>.

This is the author's peer reviewed, accepted manuscript. However, the online version of record will be different from this version once it has been copyedited and typeset.
PLEASE CITE THIS ARTICLE AS DOI: 10.1063/5.0077916

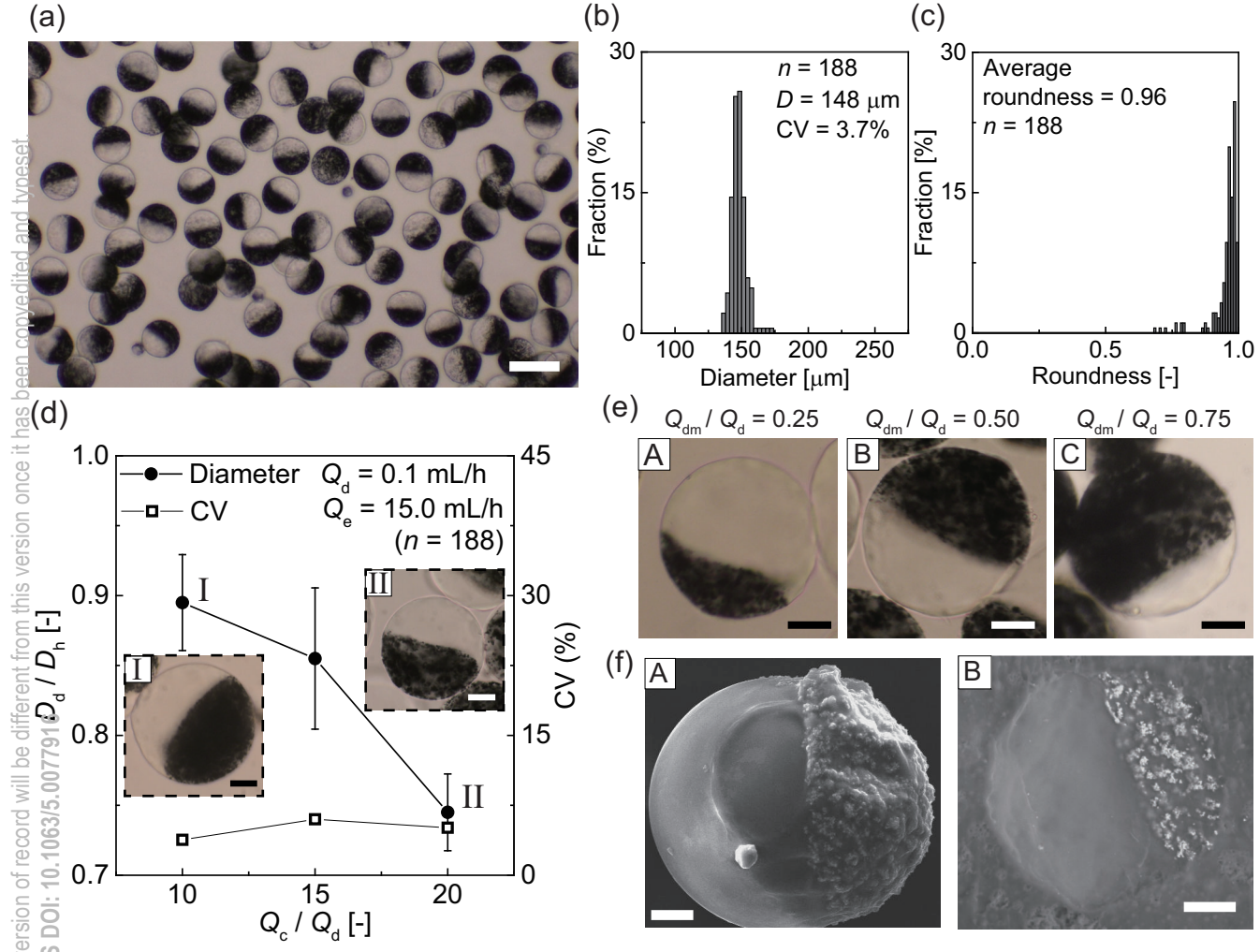


This is the author's peer reviewed, accepted manuscript. However, the online version of record will be different from this version once it has been copyedited and typeset.
 PLEASE CITE THIS ARTICLE AS DOI: 10.1063/5.0077916

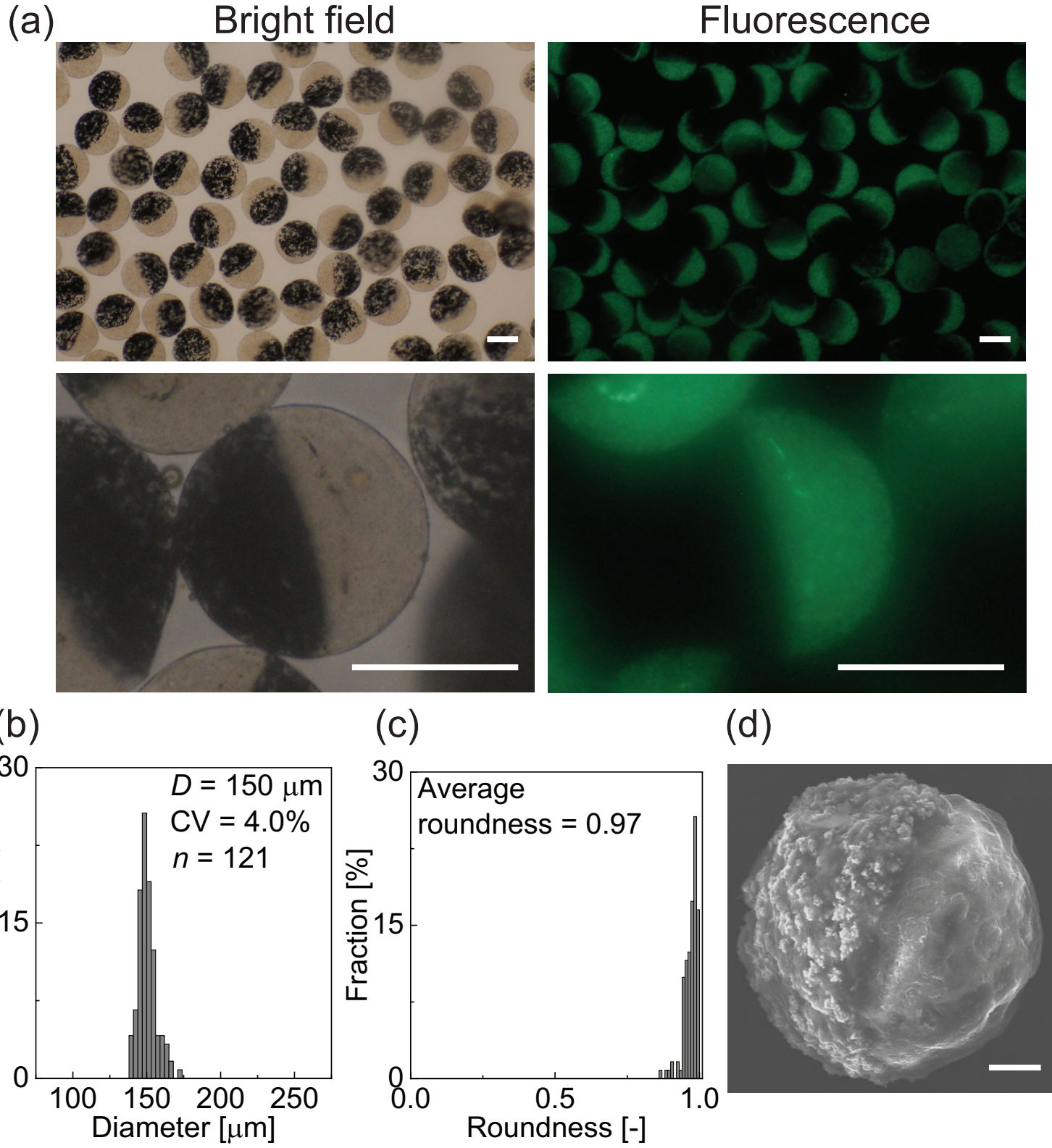


This is the author's peer reviewed, accepted manuscript. However, the online version of record will be different from this version once it has been certified and finalized.

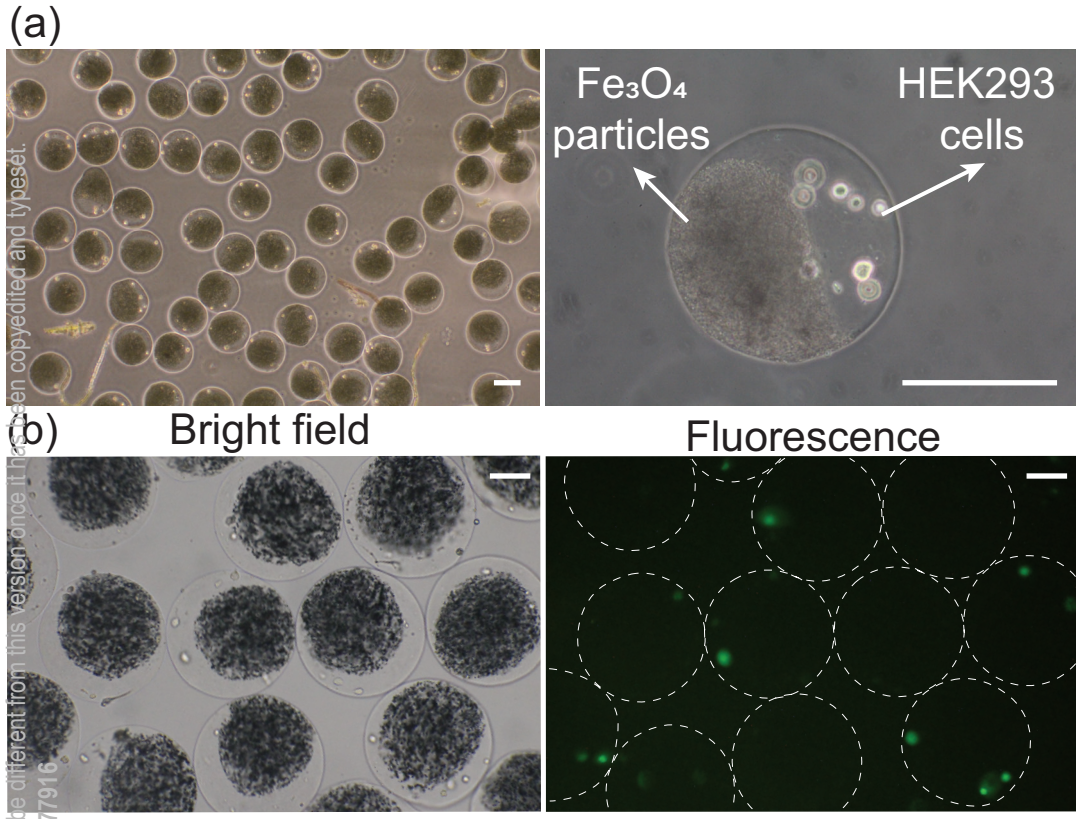
PLEASE CITE THIS ARTICLE AS DOI: 10.1063/5.0077911



This is the author's peer reviewed, accepted manuscript. However, the online version of record will be different from this version once it has been copyedited and typeset.
 Fraction (%) IS ARTICLE AS DOI: 10.1063/5.0077916



This is the author's peer reviewed, accepted manuscript. However, the online version of record will be different from this version once it has been copyedited and typeset.
 PLEASE CITE THIS ARTICLE AS DOI: 10.1063/5.0077916



This is the author's peer reviewed, accepted manuscript. However, the online version of record will be different from this version once it has been copyedited and typeset.
 PLEASE CITE THIS ARTICLE AS DOI: 10.1063/5.0077916

